J Mater Sci: Mater Med (2015) 26:138
DOI 10.1007/s10856-015-5473-8

Iron and iron-based alloys for temporary cardiovascular applications

A. Francis · Y. Yang · S. Virtanen · A. R. Boccaccini

Received: 26 November 2014 / Accepted: 20 January 2015 / Published online: 26 February 2015

Abstract In the last decade, biodegradable metals have emerged as a topic of interest for particular biomedical applications which require high strength to bulk ratio, including for cardiovascular stents. The advantages of biodegradable materials are related to the reduction of long term risks associated with the presence of permanent metal implants, e.g. chronic inflammation and in-stent restenosis. From a structural point of view, the analysis of the literature reveals that iron-based alloys used as temporary biodegradable stents have several advantages over Mg-based alloys in terms of ductility and strength. Efforts on the modification and tunability of iron-based alloys design and compositions have been mainly focused on controlling the degradation rate while retaining the mechanical integrity within a reasonable period. The early pre-clinical results of many iron-based alloys seem promising for future implants developments. This review discusses the available literature focusing mainly on: (i) Fe and Fe-based alloys design and fabrication techniques; (ii) in vitro and in vivo performance; (iii) cytotoxicity and cell viability tests.

A. Francis (✉)
Department of Advanced Materials, Central Metallurgical R&D Institute (CMRDI), P.O. Box 87, Helwan, Cairo, Egypt
e-mail: adel_francis@hotmail.com

Y. Yang · A. R. Boccaccini (✉)
Department of Materials Science and Engineering, Institute of Biomaterials, University of Erlangen-Nuremberg, Cauerstrasse 6, 91058 Erlangen, Germany
e-mail: aldo.boccaccini@ww.uni-erlangen.de

S. Virtanen
Department of Materials Science and Engineering, Institute of Surface Science and Corrosion, University of Erlangen-Nuremberg, 91058 Erlangen, Germany

1 Introduction

For the past 25 years, the cardiovascular stent technology has been based on the long-term (permanent) need of stent function with 316L stainless steel, titanium and cobalt–chromium alloys as materials of choice. These metallic materials are widely used in medical implants, owing to their high strength, biological performance, ductility and good corrosion resistance [1]. However, permanent (long-term) implantation of a metallic stent in an artery can lead to clinical complications such as thrombosis, in-stent restenosis, prolonged physical irritations, chronic inflammation, and stent fracture. To mitigate or avoid the aforementioned complications, the concept of temporary biodegradable cardiovascular metal implants was introduced as a way-out to these downsides. The two main materials used in biodegradable stents are polymers and metals. In comparison to polymer biodegradable stents which have demonstrated some limitations such as local inflammation, radiolucency, limited mechanical performance and early recoil post implantation [2, 3], metal stents are remarkable since they have the potential to perform similarly to traditional stainless steel metal stents.

So far, two types of biodegradable metal alloys (iron and magnesium-based alloys) have emerged as a interesting materials for specific applications which require high strength to bulk ratio such as in coronary stents. In this context, the degradation products of both metallic materials are biocompatible, partially remaining intact for several months before completion of vascular healing [4], allowing restoration of vasoreactivity with the potential of vessel remodeling [5], and are eventually eliminated from the body. The first clinical trial to test the feasibility and safety of the magnesium alloy (WE-43-Biotronik, Berlin, Germany) stent in humans was performed in 2007 [6].However, the rapid degradation rate of

Mg and many of its alloys within 2–3 months following implantation [7] may lead to the evolution of hydrogen gas at the interface between the surrounding tissue and the implant [8–10]. Therefore, iron-based materials are considered an interesting option for novel biodegradable coronary artery stents due to their appropriate ductility and strength compared with their counterparts, magnesium alloys. Moreover, the properties of Fe alloys could be further enhanced by purposeful alloying and by applying specific thermo-mechanical treatments [11]. Recently, an alternative approach has been launched [12, 13] to develop Fe-based materials with improved degradation behavior and bioactivity for bone implant applications by incorporating various bioactive bioceramics such as hydroxyapatite, tricalcium phosphate, biphasic calcium phosphate and calcium phosphate/chitosan.

This review will comprehensively discuss current scientific literature in the field of biodegradable iron and iron-based alloys as potential candidates for short-term (temporary) implant/stent applications and for cardiovascular intervention. Conventionally, a coronary or cardiac stent is a tiny, expandable tubular scaffold made of medical-grade and corrosion resistant stainless steel or cobalt–chromium alloy designed to open a blood vessel that is blocked by plaque. Stents can reduce the obstruction at the implantation site and prevent the narrowing or the lumen shrinkage after angioplasty procedure that is performed for patients with cardiovascular disease. The procedure involves inserting a medical device, a balloon to open the artery narrowed by plaque. A tubular mesh stent is usually placed to help maintain the vessel open (http://www.bostonscientific.com/lifebeat-online). A schematic diagram illustrating the process of opening a clogged artery is shown in Fig. 1.

Iron is distinguished from other metallic materials by its biodegradable and predominantly non-toxic properties as well as its radio-opaqueness so that addition of markers to make the stent visible by fluoroscopy is not required. Iron is also an essential co-factor for a multitude of enzymes involved in diverse physiological processes such as oxygen binding, DNA synthesis and redox enzyme activity [14]. Using a corrodible stent made of iron, Peuster et al. [15] conducted a 12-month study into the descending aorta of 29 mini-pigs. Despite the death of two animals after the implantation, the histopathological examination of heart, lung, spleen, liver, kidney and para-aortic lymphatic nodes of the remaining 27 mini-pigs demonstrated no signs of iron overload or iron-related organ toxicity. Figure 2 shows a typical iron stent investigated by Peuster et al [15].

Similarly; degradable cardiovascular Fe stents (NOR-I),implanted into the native descending aorta of 16 New Zealand white rabbits, showed a combination of low thrombogenicity and minimal inflammatory response during the follow up of 6–18 months [16]. This study was the first of its kind to test the feasibility and safety of the iron bio-corrodible stent without periprocedural complications. Figures 3 and 4 display rabbit aorta with degradable iron stent after 6 and 18 months respectively [16]. It should be pointed out that the low degradation rate of pure iron in physiological media might reveal reactions similar to those found in long-term stent applications and consequently this effect can lead to clinical problems. Therefore and in order to expedite the degradation process, new kinds of Fe-based materials with appropriate properties for medical applications have been developed by modifying the chemical composition and microstructure. Based on the work of Hermawan et al. [17] and Schinhammer et al. [18], an ideal strategy for biodegradable Fe-based alloy stent should demonstrate a compromise between degradation and mechanical integrity. It is reported that the most favorable and suitable stent should maintain its mechanical integrity for the first 6–12 months but be totally degraded after 12–24 months. This review will mainly focus on concepts and technology of biodegradable Fe-based structures (stents) aiming at gaining an overview of the biodegradability, cytotoxicity and in vivo/in vitro behavior of Fe and Fe-based biodegradable materials. The fabrication techniques and biocompatibility of iron-based alloys with an emphasis on viability tests and cell proliferation are also reviewed.

2 Alloying elements

Several types of iron-based alloys have been proposed for cardiovascular stent applications, including pure iron metal, binary Fe-metal alloys (metal = Mn, Co, Al, W, Sn, B, C, S, Pd and Pt), Fe–10Mn–1 % Pd [19], Fe–21Mn–0.7C (labeled TWIP), Fe–21Mn–0.7C–1 % Pd (labeled TWIP-1Pd) [20], Fe–Mn–Si [21], and Fe-based bulk metallic glasses (BMG) [22]. Suitable alloying elements for iron biomaterials must fulfill the requirements of temporary implant applications without neglecting the favorable combination of high strength, appropriate corrosion rate and good biocompatibility. The selection of Mn in the Fe–Mn alloy system was justified by its essentiality for the body function of all mammals, even though its excess is not reported to be toxic in cardiovascular systems [23, 24]. On the basis of this analogy, $Fe_{30}Mn_6Si$ alloy [21] has been developed as a biodegradable metal candidate, since element Si is found in the human body. On the other hand, the suitability of the Fe–Pd (Pt) [4] alloys for biodegradable vascular stents relies on their excellent biocompatibility and the mismatch of their standard electrode potentials (Pd: −0.126 V vs. SHE, Pt: 1.2 V vs. SHE) with iron (Fe: −0.44 V vs. SHE) which can accelerate the degradation of pure iron (this is of interest, since the corrosion rate of pure Fe in the biological environment seems to be too slow for biodegradable implant applications).

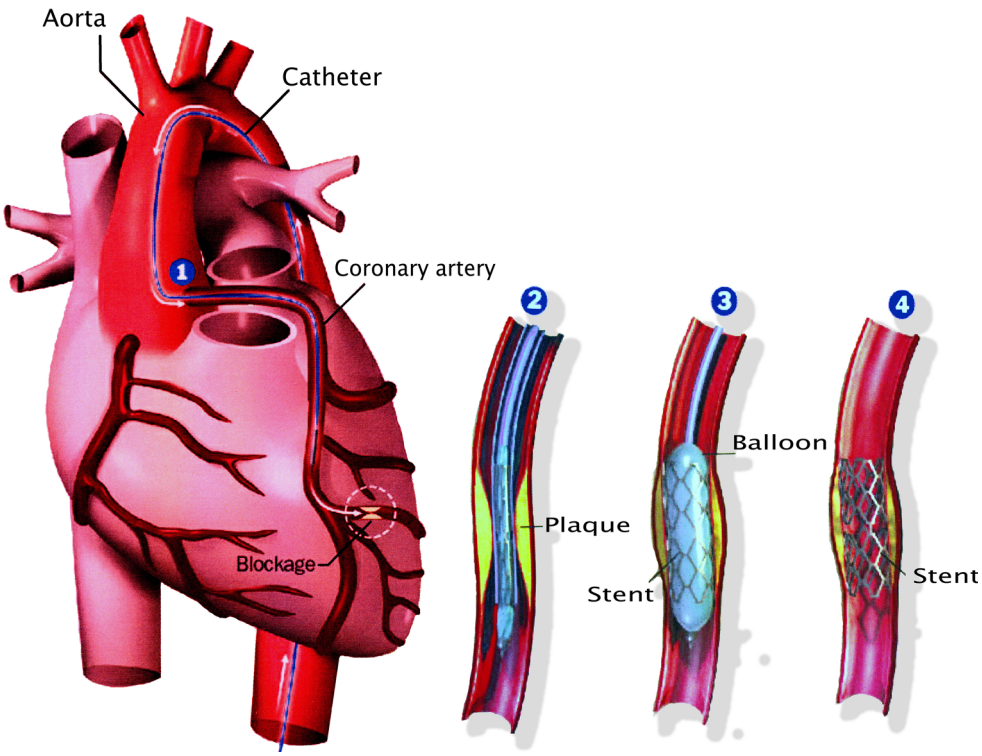

Fig. 1 Schematic diagram illustrating the process of opening a clogged artery. *1* A catheter is inserted through an artery in the groin and passed into the heart where a dye is released to identify blockages, *2* a balloon inside the stent is introduced into the blockage, *3* When the balloon is inflated, the stent expands, *4* the balloon is deflated and withdrawn, the stent holds the artery open. Diagram by Michel Gabra, inspired from http://www.joelertola.com/grfx/stent/stent.html

Fig. 2 Photograph of an iron stent in the design of a peripheral Saxx stent (CR Bard, Tempe, AZ, USA) prior to mounting on the balloon catheter. After laser-cutting and electropolishing the stent had a strut thickness and length of 120 μm and 20 mm respectively (Reproduced with permission of Elsevier from Ref. [15])

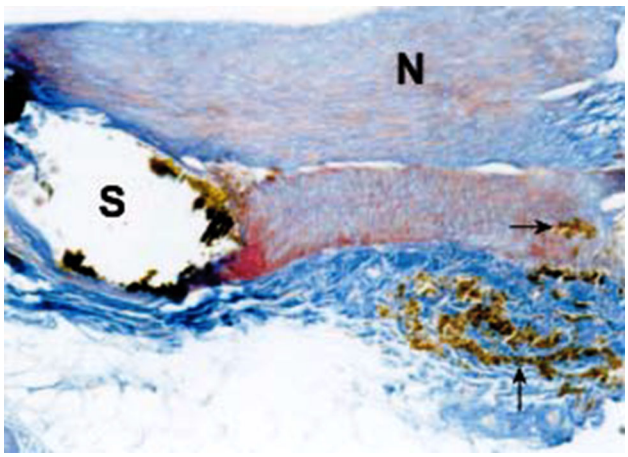

Fig. 3 Rabbit aorta with degradable iron stent 6 months after implantation. The stent struts are lost and iron remnants are visible as plaques of *brownish* pigment. The stent strut is seen to be covered by neointima (N). Accumulation of iron laden macrophages within the media and adventitia (*arrow*). Azan stain, original magnification ×10 (Reproduced with permission of **BMJ Publishing Group Ltd** from Ref. [16]) (Color figure online)

3 Materials and manufacturing techniques for fabrication of iron-based alloys

Casting has marked advantages in the production of complex shapes and it is primarily used in the manufacturing process of surgical metallic materials including stents. Melting of metals is always performed under vacuum condition and the resulting product is subsequently subjected to various forming and thermo-mechanical processes to achieve the desired shape and mechanical properties required for the particular application [25–27]. The vacuum technique in melting operations is not only used to minimize or avoid the formation of inclusions but also to remove occluded or dissolved gases from the bulk of

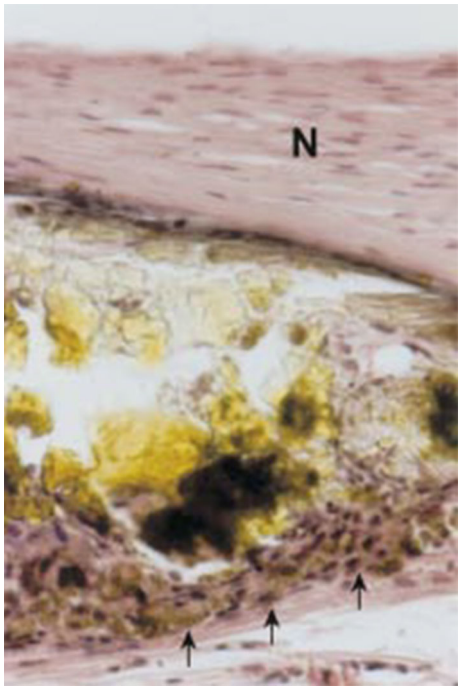

Fig. 4 Rabbit aorta with degradable iron stent 18 months after implantation. A stent strut is seen to be covered by neointima (N) and along the adventitial side there is moderate infiltration of macrophages (*arrows*) is observed. Haematoxylin and eosin stain, original magnification ×40. (Reproduced with permission of **BMJ Publishing Group Ltd** from Ref. [16])

material. With the objective of maximizing reliability and performance of iron-based alloys for clinical applications, the metallurgy of the specific alloy should be considered to achieve the optimum properties (corrosion resistance, ductility, fatigue and fracture resistance, strength, workability and machinability) for the desired application. Different fabrication techniques are introduced to manufacture new kinds of degradable iron-based materials.

3.1 Vacuum induction furnace

The following alloys with the nominal compositions Fe–10Mn, Fe–10Mn–1 % Pd [19], Fe–21Mn–0.7C (labeled TWIP), Fe–21Mn–0.7C–1 % Pd (labeled TWIP-1Pd) [20], and Fe–30Mn–6Si [21] were produced from their raw elements after melting and casting in a vacuum induction furnace under argon atmosphere. To ensure homogenization, the ingots were encapsulated in quartz tubes under a 215 mbar argon atmosphere and solution-heat-treated (SHT) for 12 h at 1250 °C, followed by water quenching [19]. Isothermal aging of the SHT specimens was performed at 375, 400, 425, 450 and 500 °C in air for various durations (up to 11 days), followed by quenching in water. However, the cylindrical ingots (diameter 75 mm), prepared by Schinhammer et al. [20], were forged at approximately 1000 °C to a diameter of 12 mm followed by solution-heat-treatment (sht) for 10 h at 1250 °C under argon atmosphere and subsequently water-quenched.

Liu et al. [28] prepared six binary iron alloy ingots for use as coronary stents. They explored the effect of the alloying elements (Mn, Co, Al, W, B, C and S) on the biodegradability and biocompatibility of pure iron. The pure elements were mixed, melted and cast in a vacuum induction furnace under an argon atmosphere with 97 at.% iron and 3 at.% alloying element. It is known that the aforementioned elements affect the mechanical and physical properties of industrial steels.

3.2 Molecular beam epitaxy

Allenstein et al. [29] employed 2 different routes to produce (i) single crystalline $Fe_{70}Pd_{30}$ thin films of 500 nm thickness on MgO (001) substrates of size 1 cm^2 by molecular beam epitaxy, and (ii) splats of the same composition by ultra-rapid quenching of 180 mg $Fe_{70}Pd_{30}$ as explained in the references [30, 31]. Splat-quenching of the alloy $Fe_{70}Pd_{30}$ was found to be an excellent method to obtain thin foils in the fcc austenite phase, which show a martensitic transformation upon cooling. Both vapor-deposited single crystalline $Fe_{70}Pd_{30}$ thin films and roughness graded polycrystalline splats of the same stoichiometry exhibit excellent biocompatibility and bioactivity in contact with different cell types.

3.3 Spark plasma sintering (SPS)

Spark plasma sintering technique was applied to prepare two composite specimens of Fe–5 % Pd and Fe–5 % Pt [4]. The sintering of pure starting powders (Fe, Pd and Pt) was carried out under vacuum at 1000 °C for a holding time of 5 min. Others [32] fabricated biodegradable Fe-X composites with typical metal W and nonmetal CNT (carbon nanotube) as the reinforcement phase by SPS to obtain a faster degradation rate of iron-based materials by microgalvanic corrosion mechanism. The sintering process was performed under a pressure of 40 MPa at 950 °C for 5 min. The presence of a suitable second phase in combination with Fe is beneficial for increasing the strength and the degradation rate of pure iron for future development of new degradable metallic stents.

3.4 Arc melting furnace

Three alloy ingots of Fe-based bulk metallic glasses (BMG) were prepared by melting appropriate atomic percentages of Fe, Co, Cr, Mo, C, B, Mn, Er and Y, in an arc-melting furnace with a non-consumable tungsten electrode and water cooled copper hearth under an ultra-pure argon atmosphere. The three kinds of alloys are $Fe_{41}Co_7Cr_{15}Mo_{14}C_{15}B_6Y_2$

(BMG1), $(Fe_{44}Cr_5Co_5Mo_{13}Mn_{11}C_{16}B_6)_{98}Y_2$ (BMG2), and $Fe_{48}Cr_{15}Mo_{14}C_{15}B_6Er_2$ (BMG3) [22]. The homogenization of the samples' composition was performed by remelting each ingot at least five times. Cylindrical shapes with diameter of 5 mm were obtained by suction casting of the molten alloys into a coppermold. The corrosion performances and cytotoxicity tests demonstrate that Fe based BMGs might open up a new path for the biomedical applications, especially in dental implantology.

3.5 Powder Metallurgy (PM)

Powder metallurgy is a simple processing tool to manufacture reliable and high purity ferrous and non-ferrous alloys. This approach has been used to produce Fe–C, Fe–0.6P, Fe–1.6P, Fe–B and Fe–Ag samples at 1050–1120 °C [33]. Hermawan et al. [34] applied also the same approach to prepare four Fe–Mn alloys, namely $Fe_{20}Mn$, $Fe_{25}Mn$, $Fe_{30}Mn$, and $Fe_{35}Mn$, from high purity elemental powder. The numbers specified the nominal weight percentage of manganese. The sintering temperature of the compacted powder mixtures was fixed at 1200 °C for 3 h in a flowing Ar-5 % H_2 gas mixture. The obtained products were then cold rolled and re-sintered to obtain high density material with aligned porosity.

3.6 Electroforming

Electroformed Fe specimens were fabricated in flat form from an aqueous solution of ferrous chloride–calcium chloride mixture. Sodium saccharine and sodium dodecyl sulfate were added to the electrolyte mixture as stress-reducing and anti-pitting agents. Ti6Al4V alloy was selected as a cathode and Armco® iron sheet was used as a soluble anode to provide Fe^{2+} ions in the electrolyte. The electrodeposition was carried out at 90 °C for 4.30 h with a direct current of 2 A dm^{-2} to produce Fe foils with the lowest surface roughness [35]. The foils were removed after deposition to be used as separate entities. Electroforming produces polycrystalline metals with exceptionally fine-grain structure with grain sizes much smaller than in bulk metals produced by other production methods.

3.7 Equal channel angular pressure (ECAP) technique

Nanocrystalline pure iron rods were fabricated from commercial pure iron (>99.8 wt%) by the equal channel angular pressure (ECAP) technique up to eight passes [36]. It should be noted that Equal channel angular pressing (ECAP) and high pressure torsion (HPT) are two severe plastic deformation (SPD) processes that have been introduced by Stolyarov et al. [37] to develop bulk nanocrystalline/nanostructured materials. The stronger corrosion resistance and durable lifespan of the nanocrystalline eighth pass ECAPed pure iron over the microcrystalline counterpart fit well as a biodegradable stent material.

4 In vitro and In vivo performance of iron and iron-based alloys

Since the introduction of stent technology in 1987, a variety of different biodegradable materials have been proposed to construct implants with prolonged and safe degradation. The concept of a stent that fulfills its main function and then is consumed and excreted by the body leaving no trace is in demand. The very low degradation rate of pure iron in physiological media has urged scientists to propose various designs of iron alloys for biomedical applications. The design strategy required to develop Fe-based alloys for biodegradable stent applications should maintain three main characteristics: (i) good strength approaching 316L SS alloy; (ii) biocompatibility (no release of toxic breakdown products), and (iii) controlled degradation rate within a reasonable period (1–2 years) [38]. For convenience, the mechanical properties of iron and iron-based alloys, including yield strength, hardness, ultimate strength and ductility are listed in Table 1.

4.1 Acellular in vitro behavior

In order to assess the early signs of cell compatibility of implants, in vitro studies should be conducted using both static (immersion in a cell culture medium) and dynamic (electrochemical) tests to evaluate the degradation behavior of the metallic implant. Hermawan et al. [34, 39, 40] were pioneers to reporting the influence of alloying elements on the performance of biodegradable iron-based materials. They developed a series of Fe–Mn alloys with the objective to obtain mechanical properties similar to those of stainless steel 316L and degradation behavior more suited than that of pure iron. The four alloys with Mn content ranging between 20 and 35 wt% were shown to exhibit higher corrosion current than that of pure iron as illustrated in their potentiodynamic polarization curves, Fig. 5. Based on their corrosion behaviors, superior ductility and relatively low strengths, $Fe_{30}Mn$ and $Fe_{35}Mn$ showed the best characteristics for biodegradable stents application.

In the light of the aforementioned study of biodegradable iron-based alloys, Liu et al. [21] investigated the feasibility of Fe–Mn–Si alloy as a potential degradable biomaterial. From an electrochemical point of view the higher corrosion rate of both $Fe_{30}Mn_6Si$ and $Fe_{30}Mn$ alloys is attributed to the presence of ε-martensite and γ-austenite phases, while α-ferrite is the single phase of pure iron which is known to be more corrosion resistant than the two phases [41].

Table 1 Mechanical properties of iron and iron-based alloys

Materials	Yield strength, MPa	Ultimate strength, MPa	Elongation % at fracture	Hardness HV/10	References
99.9 % Fe (Armco)	250	300	37.5	85 ± 1	[18]
Nanocrystalline Fe:ECAP, 8 passes	470 ± 29	–	–	(Microhardness = 444 ± 31 kgF/mm^{-2})	[36]
Fe (carbon steel, Sht)	700	900	9.5	403 ± 2	[18]
Fe–10Mn (Sht)	NA	NA	NA	428 ± 6	[18]
Fe–10Mn (ht 1)[c]	800	1400	14	384 ± 5	[18]
Fe–10Mn (ht 2)[c]	650	1300	14	374 ± 7	[18]
Fe–10Mn–1Pd (Sht)[b]	950	1500	2	432 ± 8	[18]
Fe–10Mn–1Pd (ht 1)	900	1550	7	437 ± 3	[18]
Fe–10Mn–1Pd (ht 2)	850	1450	11	376 ± 6	[18]
Fe–20 % Mn	421 ± 27	702 ± 11	7.5 ± 1.5	230 ± 1	[34]
Fe–25 % Mn	361 ± 33	723 ± 19	4.8 ± 0.4	200 ± 1	[34]
Fe–30 % Mn	239 ± 13	518 ± 14	19 ± 1.4	110 ± 1	[34]
Fe–35 % Mn	234 ± 7	428 ± 7	32 ± 0.8	106 ± 2	[34]
Fe–21Mn–0.7C (TWIP)-ReXX	345 ± 10	980 ± 5	62 ± 4		[20]
TWIP-1Pd(Rexx)[a]	360 ± 4	970 ± 35	64 ± 3		[20]
TWIP-1Pd CW12[a]	690 ± 35	1120 ± 25	38 ± 3		[20]
TWIP-1Pd CW12-ht[a]	505 ± 20	1020 ± 10	53 ± 7		[20]
TWIP-1Pd CW23[a]	1095 ± 35	1320 ± 15	29 ± 2		[20]
TWIP-1Pd CW23-ht[a]	725 ± 20	1255 ± 15	38 ± 2		[20]
Stainless steel (316 L SS)	190	490	40		[34]
Pure iron, annealed plate	150	210	40	119 ± 3 (HV 0.2/10)	[34]
Co–Cr alloys (ASTM F90)	310	860	20		[55]
Mg, as cast	20	86	13		[5, 56]
Fe–5 % Pd	445 ± 13	754 ± 20	–	184 ± 10 (HV0.2/10)	[4]
Fe–5 % Pt	503 ± 22	785 ± 18	–	309 ± 8 (HV0.2/10)	[4]
Electroformed iron	360 ± 9	423 ± 12	8.3 ± 2		[35]
Electroformed iron annealed at 550 °C	270 ± 6	292 ± 14	18.4 ± 4		[35]
Electroformed iron annealed at 600 °C	130 ± 7	169 ± 9	32.3 ± 5		[35]
Pure iron annealed at 550 °C	140 ± 10	205 ± 6	25.5 ± 3		[35]
WE43 Mg alloy	162	250	2		[35, 57]
Fe–30Mn–6Si alloy: solution treated	180	450	16		[21]
Fe alloyed by different elements (Mn, Co, Al, W, Sn, B, C and S): as cast	100–220	190–360	12–23		[28]

Mg and Co–Cr alloys are only cited for comparison purposes

Pure iron (99.8 %), annealed plate, as provided by Goodfellow Corporation, Oakdale, PA, USA

ECAP equal channel angular pressure

[a] *TWIP* twinning induced plasticity, *Rexx* recrystallization, *CW* subjected to 12 or 23 % cold working, *ht* annealed for 30 min at 700 °C

[b] *Sht* solution heat treated at 1000 °C for 2 h under Argon and subsequently water quenched

[c] *ht 1* aged for 1 h at 500 °C in Air, *ht 2* annealed 10 min at 700 °C and then annealed for 10 h at 500 °C

Table 2 summarizes the data of the potentiodynamic polarization (corrosion current density I_{corr}; corrosion potential E_{corr}) for various iron and iron-based alloys.

In an effort to accelerate the degradation rate of iron stents and keeping sufficient mechanical strength to support the healing process, more complex alloying

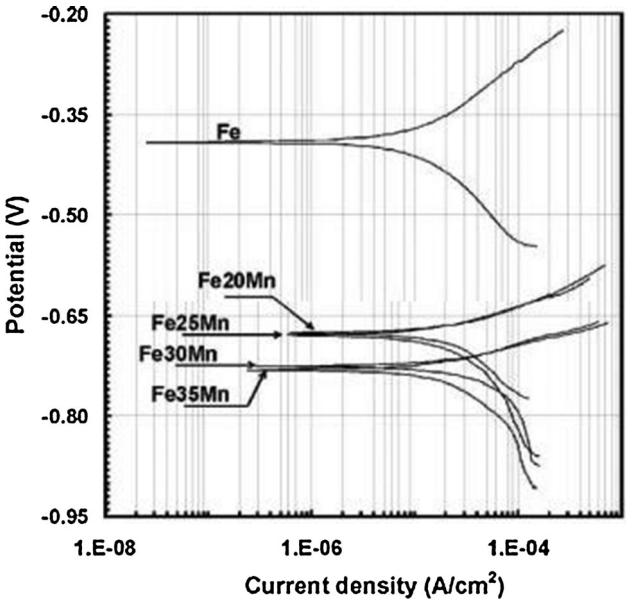

Fig. 5 Polarization curves of pure iron and quenched Fe–Mn samples containing 20, 25, 30 and 35 wt% Mn. (Reproduced with permission of **John Wiley and Sons** from Ref. [34])

compositions containing very small levels of noble metals (Pd, Pt) may be necessary. These noble metal containing alloys exhibit good mechanical properties and degradation behavior as well as good biocompatibility. Huang et al. [4] report that iron alloyed with 5 wt% Pd or Pt showed faster corrosion rates than that of as-cast pure iron and even better than Fe–0.5 wt% CNT and Fe–5 wt% W [32]. Figure 6 displays the corrosion rates calculated from the weight loss of samples after static or dynamic immersion in Hank's solution for 30 days. In addition to galvanic corrosion, the presence of ferrous oxide in Fe–Pd and Fe–Pt composites should not be neglected as a reason for increasing corrosion rate. Moreover, the micro-hardness of both Fe–Pd and Fe–Pt composites was much higher than that of pure iron (119 ± 3 HV0.2/10) which means that the addition of Pd or Pt greatly enhanced the strength of iron matrix.

It has been found [35] that the degradation behavior of Fe-base alloys depends on the processing technique. Meanwhile, the degradation rate of Fe–Mn alloys produced by powder metallurgy had a faster in vitro degradation compared to the same alloy produced by casting, as the PM process produces more porosity than the casting one. Similarly, electroformed iron also showed a faster in vitro degradation compared to Armco® Fe fabricated by casting, since the electroformed material had a much finer microstructure with increased volume of grain boundaries which are more susceptible to corrosive attack [42].

On the other hand, other investigators [18] rely on the controlled modification of the microstructure of iron by suitable alloying (Mn, Pd) and appropriate heat treatment parameters. The first alloying element (Mn) makes the Fe matrix more susceptible to corrosion through the formation of a solid solution, while the second one (Pd) generates small and finely dispersed intermetallic phases (IMPs) that act as cathodic sites towards the Fe matrix, inducing micro-galvanic corrosion. Compared to the Fe–Mn system or carbon steel, the results of the EIS measurements in SBF (Fig. 7) reveal that the newly developed Fe–10Mn–1Pd alloy in differently aged conditions (ht 1 and ht 2) exhibit lower polarization resistances [18].

To further explore the degradation performance of Fe-based alloys, the austenitic Fe–21Mn–0.7C–(1Pd) alloys designated as TWIP and TWIP-1Pd offer an attractive combination of degradation rate and mechanical characteristics for biodegradable medical applications [43]. The plot of the polarization resistance (R_p), which is a measure of corrosion tendency as a function of the immersion time reveals clear differences between the alloys (Fig. 8) [43]. The highest polarization resistance was found for the Fe samples. The TWIP samples show R_p values that are lower by a factor of approximately four. The lowest polarization resistances were found for the TWIP-1Pd samples.

The light optical image (Fig. 9a) of TWIP-1Pd CW12-700C sample after immersion for 24 h in SBF shows the localization of the corrosion attack and nucleation of pits at the surface. However, The SEM image (Fig. 9b) reveals the coverage of the entire surface with a thin layer of degradation products [43].

The degradation mechanism of Fe-based alloys process and formation of degradation products is schematically illustrated in Fig. 10, where the released metal ions react with the hydroxyl-ions to form hydrous ferrous oxide ($FeO{\cdot}nH_2O$) or ferrous hydroxide ($Fe(OH)_2$) [43]. This degradation process could be applied for all iron-containing alloys. Recently, Liu et al. investigated the effects of alloying elements (Mn, Co, Al, W, Sn, B, C, and S) on the biodegradability and biocompatibility of pure iron [28].The results showed that the elements Co, W, C, and S are suitable as alloying elements for iron-based biomaterials based on a comprehensive consideration of the improved mechanical properties, appropriate corrosion rates and good biocompatibility. With the aim to increasing the degradation rate of iron, an electroforming process was applied to fabricate pure iron for degradable stents [42].The newly formed Fe was more prone to degradation because of the fine grains and microstructural defects, which resulted in the release of a higher quantity of Fe^{2+}. The corrosion mechanism of electroformed iron appeared to be uniform as no localized attack was observed after the degradation testing.

Table 2 Potentiodynamic polarization results of pure Fe and iron-based alloys

Materials	i_{Corr} (μAcm^{-2})	Corrosion potential (mV)	Media	References
Electroformed iron (E–Fe)	73.4 ± 4.2	−824 ± 18	Hank's solution	[35]
(E–Fe) annealed	44.3 ± 5.8	−776 ± 20	Hank's solution	[35]
CTT-Fe annealed	14 ± 1.3	−732 ± 16	Hank's solution	[35]
Pure iron	8.961	−748	Hank's solution	[34]
Nanocrystalline Fe:ECAP, 8 passes	1.66 ± 0.09	600 ± 8	Hank's solution	[36]
Fe–Mn (as cast)	9.003	−711	Hank's solution	[28]
Fe–Co (as cast)	10.966	−713	Hank's solution	[28]
Fe–Al (as cast)	9.538	−704	Hank's solution	[28]
Fe–C (as cast)	15.964	−680	Hank's solution	[28]
Fe–W (as cast)	12.89	−717	Hank's solution	[28]
Fe–B (as cast)	14.962	−698	Hank's solution	[28]
Fe–20Mn (Quenched)	113 ± 4	~680	Hank's solution	[34]
Fe–25Mn (Quenched)	91 ± 4	–	Hank's solution	[34]
Fe–30Mn(Quenched)	56 ± 5	–	Hank's solution	[34]
Fe–35Mn (Quenched)	37 ± 4	~740	Hank's solution	[34]
Fe–30Mn–6Si (solution treated)	24.69	−830	Hank's solution	[21]
As cast pure iron	0.652	−387	Hank's solution	[32]
Pure iron by SPS	1.368	−400	Hank's solution	[32]
Fe–5 % Pd	1.550 ± 0.120	−471 ± 10	Hank's solution	[4]
Fe–5 % Pt	6.698 ± 0.370	−545 ± 8	Hank's solution	[4]
Fe–2 % W	6.392	−643	Hank's solution	[32]
Fe–5 % W	12.05	−556	Hank's solution	[32]
Fe–0.5 % CNT	8.397	−631	Hank's solution	[32]
Fe–1 % CNT	9.636	−667	Hank's solution	[32]
316L SS	0.454 ± 0.070	−260 ± 0.03	Hank's solution	[22]
	0.176 ± 0.041	−230 ± 0.02	Artificial saliva solution	[22]
BMG 1	0.234 ± 0.053	−270 ± 0.01	Hank's solution	[22]
	0.048 ± 0.016	−320 ± 0.02	Artificial saliva solution	[22]
BMG 2	0.288 ± 0.119	−230 ± 0.03	Hank's solution	[22]
	0.071 ± 0.039	−290 ± 0.04	Artificial saliva solution	[22]
BMG3	0.09 ± 0.017	−300 ± 0.07	Hank's solution	[22]
	0.003 ± 0.001	−250 ± 0.02	Artificial saliva solution	[22]

CTT-Fe pure iron made by casting and thermo mechanical treatment, *ECAP* equal channel angular pressure

The comparison between the degradation/corrosion rate of various iron and iron alloys in Hanks and SBF solution is presented in Fig. 11. It is clearly shown that the Fe–Mn alloy family in addition to E–Fe and Fe–5 % Pt possess the highest degradation rate. The degradation rate was calculated based on the weight loss of specimens according to the following equation [44]:

$$DR = 8.76\ x10^{4} W/A.t.\rho$$

where DR is the degradation rate in mm $year^{-1}$, W is weight loss (g), A is area (cm^2), t is time of exposure (h), and ρ is the material density (g/cm^3).

4.2 In-vivo behavior

During the last 15 years, at least four in vivo studies on metallic Fe and Fe-based alloys implants were published. These important studies have become an urgent topic in the field cardiovascular and osteosynthesis applications. In the study discussed above, for example, Peuster et al. [16] demonstrated, with an extended angiographic follow-up of 18 months, that the presence of a degradable iron stent in the descending aorta of rabbits does not seem to be associated with inflammation, neointimal proliferation, or thrombotic events during the follow-up period. In fact, histopathological

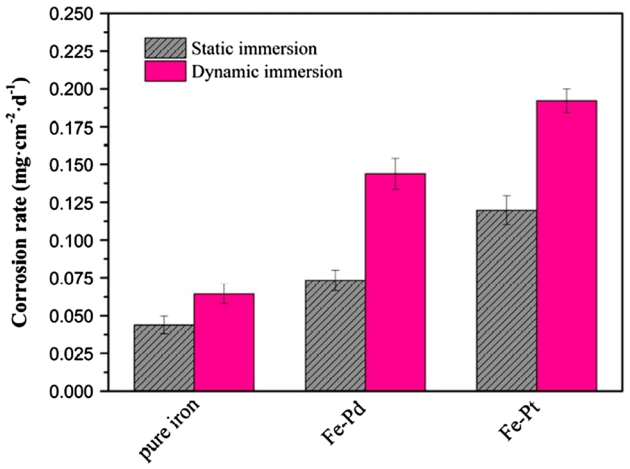

Fig. 6 Corrosion rates calculated from the weight loss of samples after static or dynamic immersion in Hank's solution for 1 month. (Reproduced with permission of Elsevier from Ref. [4])

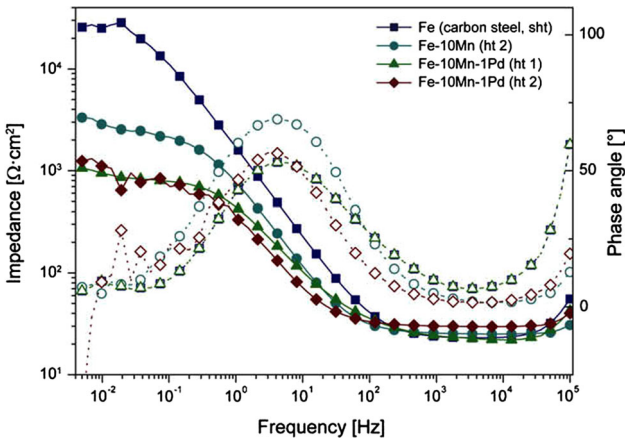

Fig. 7 Bode plots displaying the impedance (*solid symbols*) and phase shift values (*open symbols*) of Fe (sht), Fe–10Mn (ht 2) and Fe–10Mn–1Pd after two different heat treatments (ht 1 and ht 2). (Reproduced with permission of Elsevier from Ref. [18])

and macroscopic evaluation of the animals' organs did not reveal any system toxicity. The degradation of iron struts, visible by loss of distinct border lines, appeared as coarse granular brownish material located in the intima and predominantly in the media of the aorta as previously shown in Figs. 3 and 4. Following on from this, the intervention of iron stent into the native descending aorta of 29 mini-pigs with a follow-up of up to 12 months [15] showed no signs of iron overload or toxicity effect on the main organs of the pigs after histopathology analysis. Others [45] confirmed the safety and feasibility of biocorrodible iron stent for short-term implantation in porcine coronary arteries, where iron stents started after 28 days to show signs of degradation without evidence of stent particle embolization or thrombosis. Recently, Kraus et al. [46] assessed the in vivo

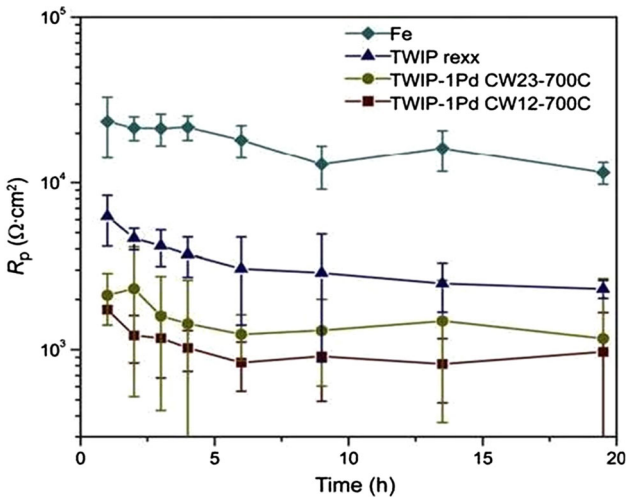

Fig. 8 Polarization resistance R_p of the degradation products as a function of immersion time in SBF solution. Fe samples exhibits the highest R_p, which is lower for TWIP and lowest for the TWIP-1Pd samples. (Reproduced with permission of Elsevier from Ref. [43])

degradation behavior of pure iron and two Fe-based alloys (Fe–10Mn–1Pd and Fe–21Mn–0.7C–1Pd) in a growing rat skeleton, where pins were transcortically implanted into the femur and monitored over a period of 1 year. No signs of local toxicity or abnormal clinical observations were noticed. The good integration of implants into the bone as well as the detection of both P and Ca on the outer layer of the degradation products is a good sign of their bioconductivity. Moreover, and in the light of the slightly higher degradation rates of the two Fe-based alloys in comparison to Fe, it was suggested that the degradation of Fe-based implants is determined mainly by in vivo conditions present in the implantation site, rather than by the composition of the material. However, the in vivo application of these alloys has not been reported in a cardiovascular context.

5 Cytotoxicity

Cytotoxicity assays are widely used to determine the response of cells to toxic substances. Various biocompatibility tests must be accomplished prior to the approval of alloy implants for in vivo studies. These tests have been often performed using MG63 osteosarcoma cells, mouse fibroblasts 3T3 and L-929 [14, 28, 36, 42, 47, 48], as well as primary cells (human umbilical vein endothelial cells (HUVECs) and mouse bone marrow stem cells. In this line, Hermawan et al. [47] stated that the relative metabolic activity of 3T3 fibroblast cells at a fixed concentration of 0.5 mg ml^{-1} in the presence of 316L SS, iron and $Fe_{35}Mn$ alloy were significantly higher than those of manganese

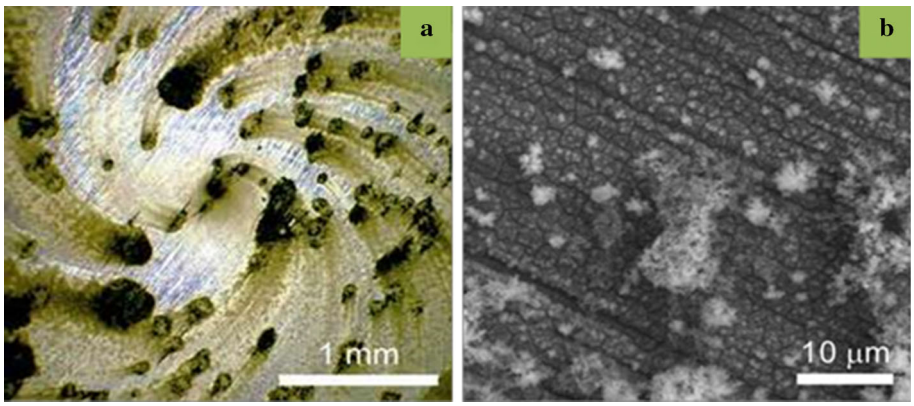

Fig. 9 Optical microscopy image of alloy TWIP-1Pd CW12-700C after 24 h in SBF. The surface depicts localized degradation. **b** The SEM image reveals the coverage of the entire sample with a layer of degradation products. (Reproduced with permission of Elsevier from Ref. [43])

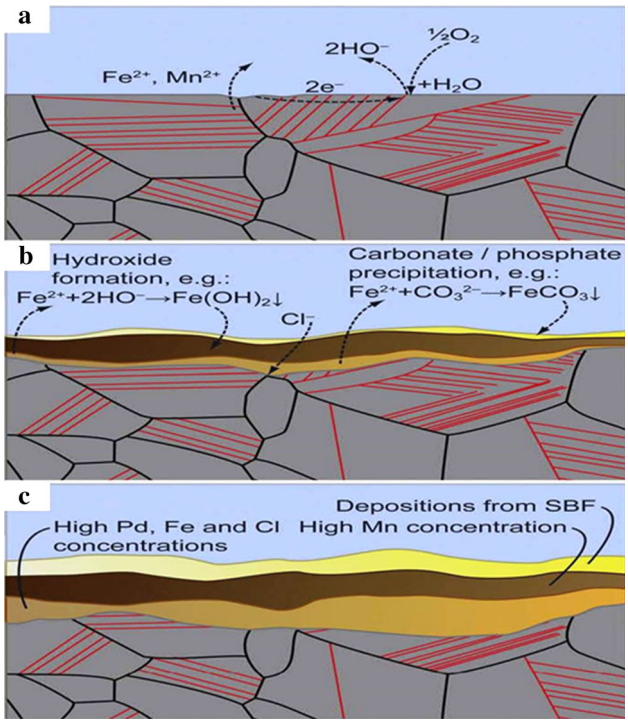

Fig. 10 Illustration showing schematically the degradation process and the formation of degradation products for TWIP-1Pd alloys. (Reproduced with permission of Elsevier from Ref. [43])

and the mixture of iron and manganese powders. However, the inhibition effect to 3T3 fibroblast cells metabolic activities increase as the concentration of the alloys in cellular medium increases.

It is a well-known [49] fact that pure Fe possesses good cytocompatibility [42] and excellent hemocompatibility [36]. However, the alloying elements such as C, Mn and Pd not only enhance the degradation rate of Fe-based alloys, but also decrease their cytocompatibility which might be due to the increased release rate of metal ions [21, 28, 47]. In vitro cytotoxicity tests using human umbilical vein endothelial cells (HUVECs) have revealed acceptable cytocompatibility based on the Fe–Mn–C (–Pd) TWIP alloys'eluates. The analysis revealed that Fe is predominantly bound in insoluble degradation products, whereas a considerable amount of Mn is in solution [49]. It was shown that Mn is the determining factor of the alloyś cytocompatibility. Wang et al. [22] investigated the indirect cytotoxicity of iron-based bulk metallic glasses as a new path for biomedical applications especially in dental implants. The results of MTT assay using L929 and NIH3T3 cells grown in Fe-based BMGs and 316L SS extracts after cell culture for 1, 2 and 4 days were quite similar and have no adverse effects on cell viability, proliferation and morphology were reported. The Fe-based BMG extract group maintained the cell viability at about 100 % during the whole incubation period. However, the cells cultured with BMG2 extract showed relatively lower values than the others except for 4-day culture. The L929 cell morphologies of Fe-based BMGs, Fig. 12, confirmed the rapid increase of cell number during the 4-day culture period for all groups [22].

Zhu et al. [14] investigated the response of human ECs to various concentrations of ferrous ions using WST-8 assay. They reported that the metabolic activity of ECs decreased at iron ion concentration ≥50 µg/ml regardless of incubation time. However, the presence of low iron concentration (<10 µg/ml) was seen to enhance the metabolic activity of ECs. In the same context [50], the response of human umbilical venous smooth muscle cells (SMCs) to an excess of ferrous ions has been assessed in a cell culture model at the phenotypic and at the molecular level. The results have led to a suggestion that high ferrous ion concentrations released from iron stents could reduce restenosis by reducing excessive vascular cell proliferation. It was also found that the gene expression level was higher for the key cell cycle regulator p53 as well as for cholesterol synthetic enzymes. This finding could be a sign of future interest to optimize the performance of iron stents, such as the application of iron chelators or inhibitors of

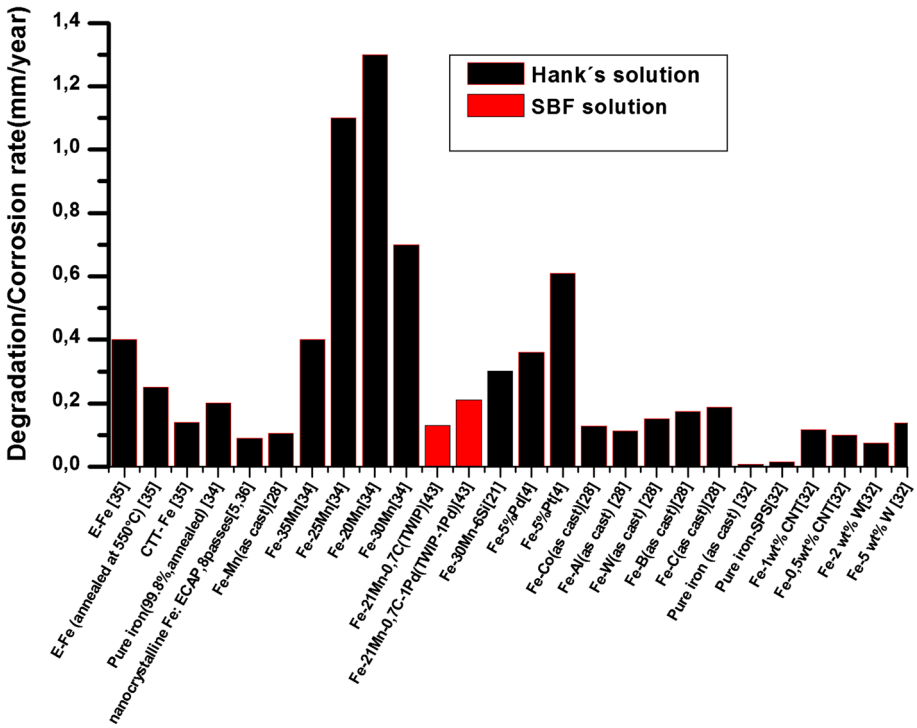

Fig. 11 Degradation/corrosion rates of iron and iron-based alloys for biomedical applications

cholesterol synthesis. p53 is a tumor suppressor protein that is induced by various cellular stress conditions, such as ionizing radiation or DNA damage [51].

In a biomechanical study to investigate the effect of alloying elements on biodegradability and biocompatibility of iron for biodegradable stents, Liu et al. [28] showed the insignificant cytotoxicity of the pure iron and Fe-X binary alloy extracts to ECV304 endothelial cells, except for the Fe–Mn alloy. Moreover, their extracts decreased the viabilities of L929 murine fibrosarcoma cells and vascular smooth muscle cells (VSMC) compared to 316L SS. Similar to the previously cited study, the same investigators assessed $Fe_{30}Mn_6Si$ as a potential biodegradable material for stents in terms of its mechanical properties, degradation, cytotoxicity and hemolysis in comparison with pure iron and $Fe_{30}Mn$ alloy [21]. This new shape memory iron-based alloy inhibits the metabolic activity of human endothelial cells (ECV304) and rodents VSMC to a higher extent compared to pure iron. Moreover, the alloy was considered to be non-hemolytic according to ASTM-F756-08 [28] as the hemolysis percentage was less than 2 %. Other authors [35, 42] used electroformed iron (E–Fe) as a structural material for biodegradable cardiovascular stent application. E–Fe showed no inhibition of the metabolic activity of primary rat SMCs compared to 316L SS and Armco® iron. However, cell counting showed a significant decrease in cell proliferation during the incubation periods for all three iron materials in comparison to 316L SS, which is primarily caused by the increased release of Fe^{2+} ions resulting from the rapid corrosion of iron, Fig. 13, [42].

In a cellular response study in which murine fibroblast cells (L-929), vascular smooth muscle cells (VSMCs) and human umbilical vein endothelia cells (ECV304) were adopted, Nie et al. [36] demonstrated that nanocrystalline pure iron, fabricated by the equal channel angular pressure (ECAP) technique up to eight passes, stimulated the proliferation of fibroblast cells more effectively and enhanced the preferable promotion of endothelialization while inhibiting the viability of VSMSc. Because of its good biocompatibility, nano-crystalline iron could be used as a novel candidate for future body implants. Figures 14 and 15 show the cell viability and morphologies after direct culture on top of the zeroth, second, fourth and eighth pass ECAPed Fe plate samples [36].

Other authors [52] explored the potential of Caveolin-1 (cav1) protein to become a biomarker for cytotoxicity after exposure to degradable metallic elements. The exposure of 3T3 mouse fibroblasts and smooth muscle cells, which have high levels of caveolins, to either ferrous and manganese ions at moderately toxic concentrations for 24 or 48 h, leads to a higher reduction of caveolins particularly in the case of manganese.

In a more recent study, Allenstein et al. [29] introduced a novel ferromagnetic shape memory alloy, Fe_{70}–Pd_{30}, as a highly promising new class of materials for medical applications, including tissue regeneration, implants, stents,

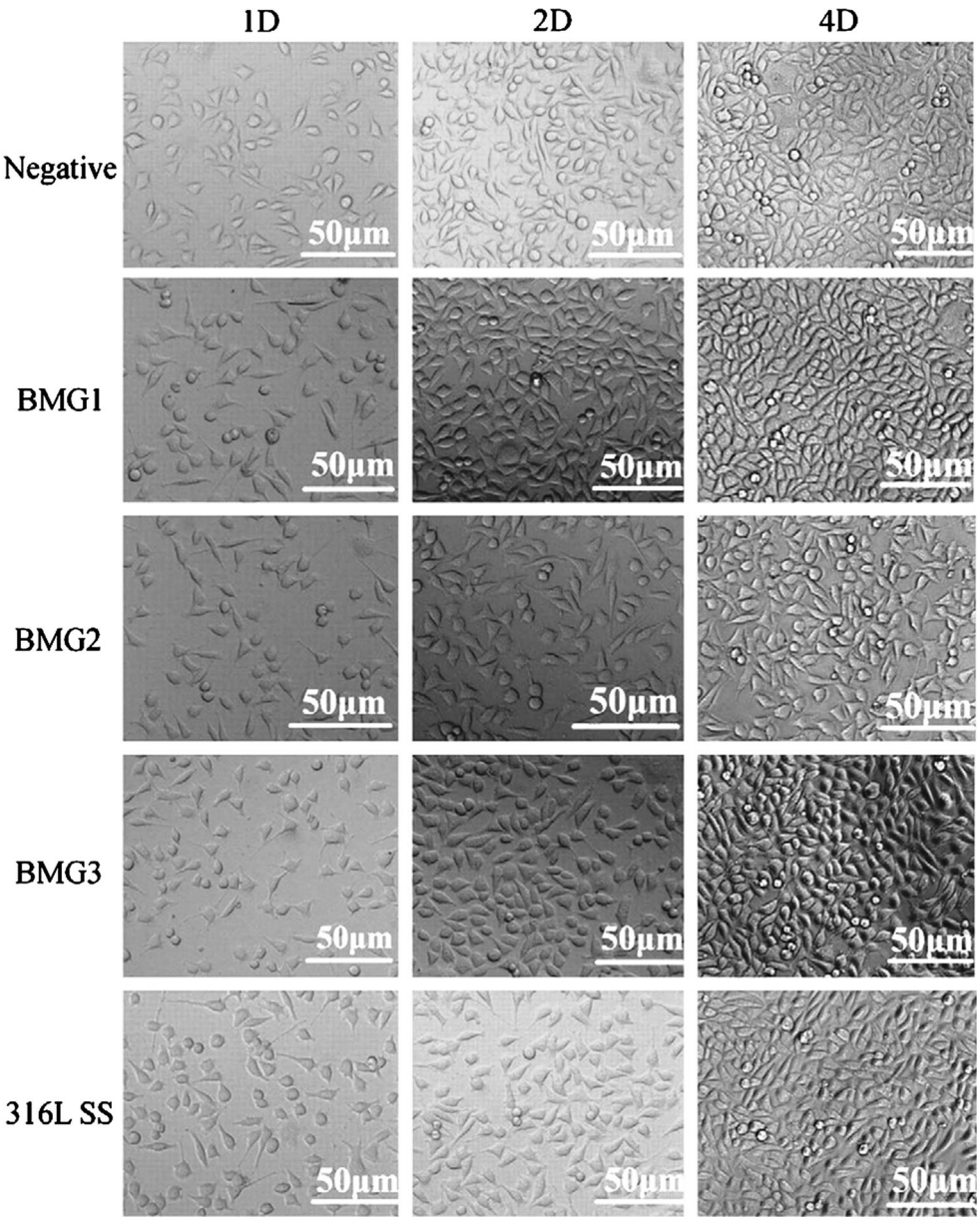

Fig. 12 Morphologies of L929 cells cultured for 1, 2, and 4 days in Fe based BMGs and 316 L SS specimen extraction media (Phase contrast microscopy). The negative group corresponds to 100 % viable cells. (Reproduced with permission of Elsevier from Ref. [22])

as well as drug delivery systems. The results of proliferation, morphology and adhesion of fibroblast (NIH/3T3) and epithelial cell lines (MCF-10A), as well as primary osteoblast cells (HOB) cultured on $Fe_{70}Pd_{30}$ thin films, demonstrated excellent biocompatibility and bioactivity features of the alloy with respect to the controls. Figure 16 shows the quantitative growth behavior of MCF-10A cells on Fe–Pd compared with that on standard plastic culture dish. It should be noted that the proliferation was modeled by an exponential increase in cellular density over time:

$\mathbf{c}(\mathbf{t}) = \mathbf{c_0 exp^{kt}}$, where c_0 is the initial concentration, t the culture time, and k the proliferation rate [29].

It was found from the inset of the afore mentioned figure that human osteoblasts (HOB) proliferate at a rate of 0.54 ± 0.04 day^{-1} on plastic and 0.59 ± 0.04 day^{-1} on $Fe_{70}Pd_{30}$ substrates, while epithelial cells (MCF-10A) e-fold 0.67 ± 0.05 times day^{-1} on plastic and 0.58 ± 0.04 times day^{-1} on Fe–Pd. Previous results of biocompatibility tests in the presence of SBF [53] showed the formation of apatite-like structures on Fe–Pd and undetectable amounts of palladium, while 0.026 mg/l of iron release was measured after 65 h, and this value matches the tolerable dose set at 45 mg/day by the Food and Nutrition Board, Institute of Medicine, USA [54].

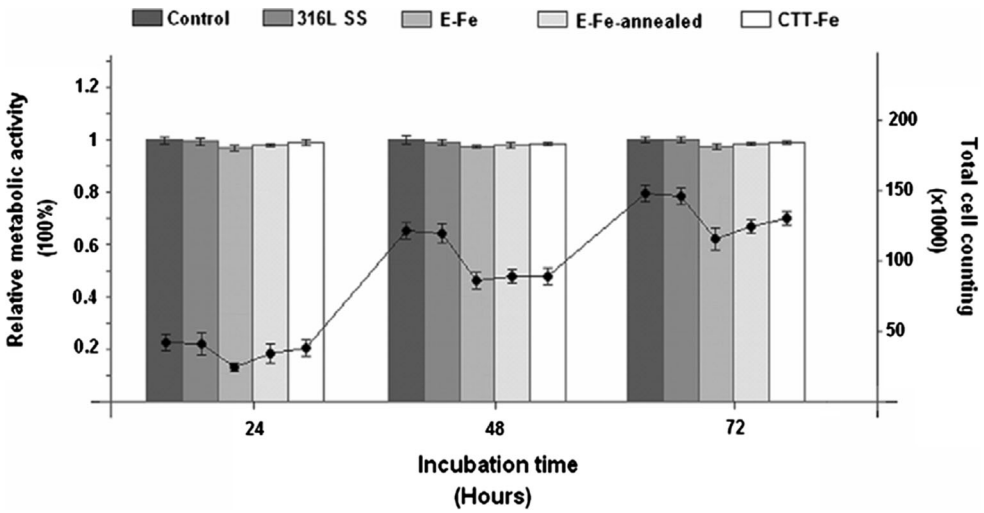

Fig. 13 Cell viability of different forms of iron and 316L SS: the column charts show cell metabolic activities as a function of incubation time at 24, 48 and 72 h (*left axis*), while the curve represents the total cell count at 24, 48, and 72 h (*right axis*). (Reproduced with permission of Elsevier from Ref. [42])

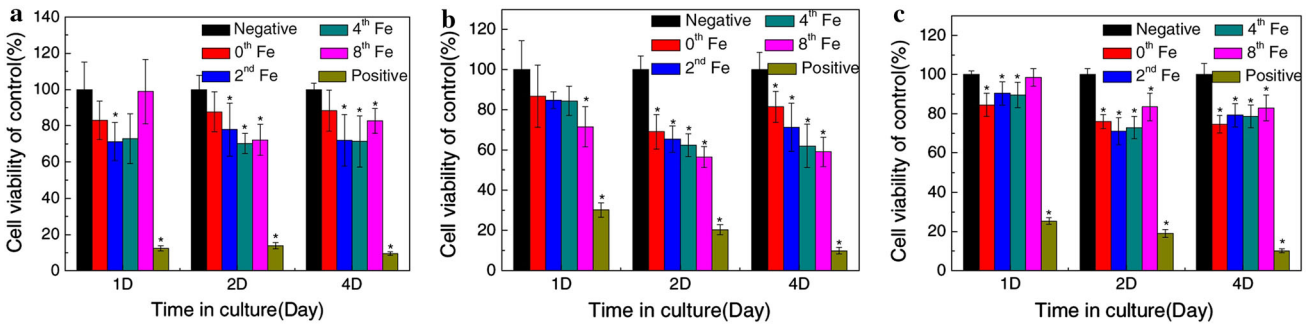

Fig. 14 Cell proliferation on pure iron samples (ECAPed) cultured with **a** L-929; **b** VSMC and **c** ECV304. Negative controls of DMEM-cultured cells and positive controls of DMSO-added cells were considered. (Reproduced with permission of IOP and corresponding author from Ref. [36])

6 Conclusions

This review has discussed the application of Fe and Fe-alloys in the cardiovascular field. The development of temporary biodegradable metallic implants in surgery and cardiovascular device applications as well as for tracheal stents and treatment of aneurisms, constitutes an active and challenging research domain in biomedicine. Metallic implants based on iron alloys combine strength, low corrosion resistance and an acceptable biocompatibility, which attract interest and promote research on these materials looking for expanding their application for optimal patient comfort. Because of their favorable biological performance and suitable interaction with the surrounding tissue, implants/stents made of iron-based materials may degrade slowly while retaining their mechanical integrity long enough to prevent early recoil. The analysis of the literature shows that the potentiality of these materials is attributed to the reduction of side effects such as chronic inflammation and in-stent restenosis, which are normally associated with permanent implants. Fundamental investigations on alloying designs should be continued to develop metallic stents with appropriate and safe degradation. Understanding the metallurgy of the specific material would obviously help to achieve final microstructures designed to produce the optimum properties and ensure safe and long-term controlled degradation when implanted in the human body. It is evident from the available literature that the performance of these alloys is highly dependent on their degradation behavior and possible cytotoxic effects of the released ions have been identified.

An ideal biodegradable implant for cardiovascular applications should feature the favorable combination of high strength and ductility with a pronounced strain hardening. The achievement of the above objectives should lead to the production of high performance and reliable biodegradable iron-based alloys with medically interesting properties which could enable also various applications in the orthopedics and other surgical fields as well as regenerative medicine in addition to cardiovascular devices.

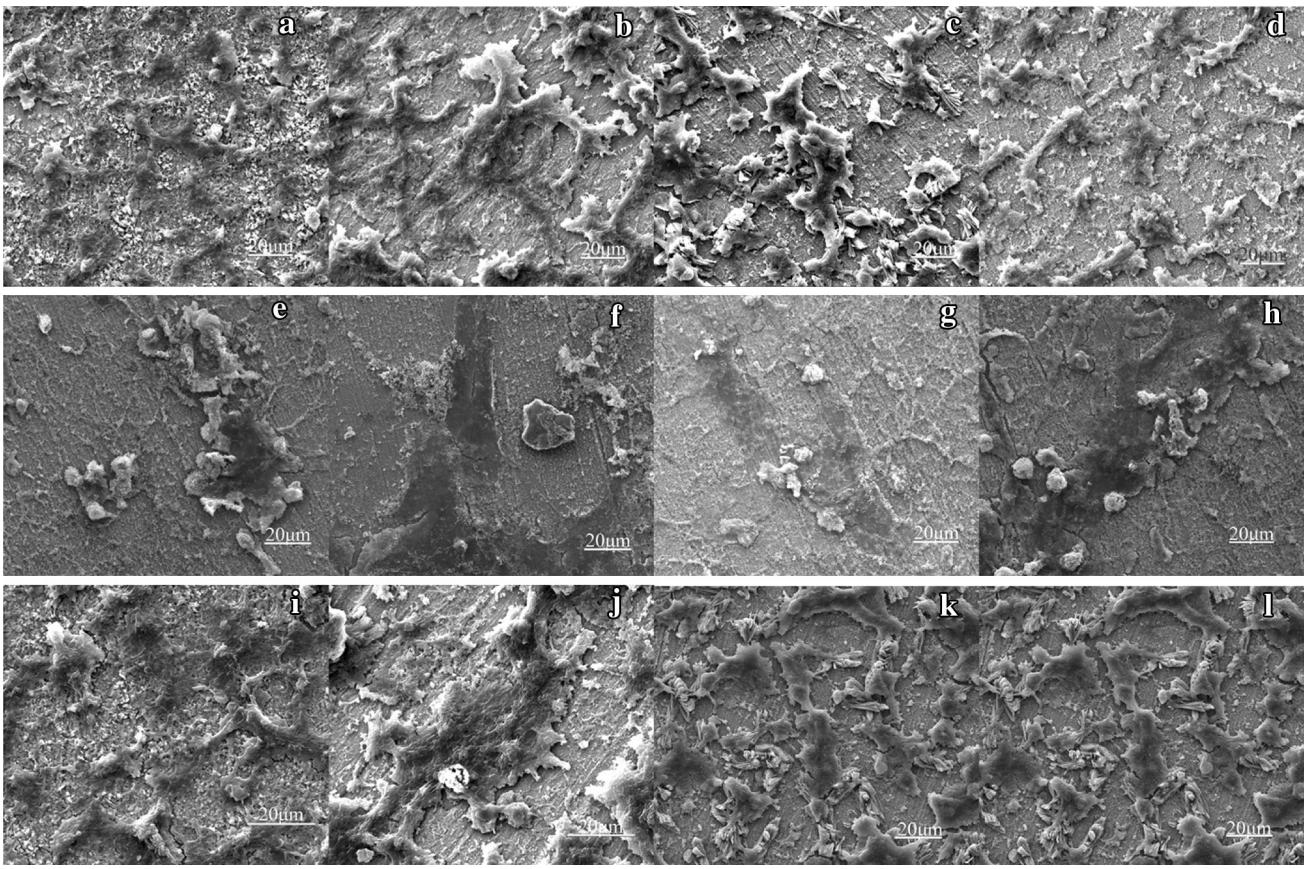

Fig. 15 SEM images showing cell attachment morphologies for different cell lines (**a**–**d** for L-929, **e**–**h** for VSMCs and **i**–**l** for ECs) on different samples (**a**, **e**, **i** for zeroth pass ECAPed Fe; **b**, **f**, **j** for second pass ECAPed Fe; **c**, **g**, **k** for fourth pass ECAPed Fe; **d**, **h**, **l** for eighth pass ECAPed Fe). (Reproduced with permission of IOP and corresponding author from Ref. [36])

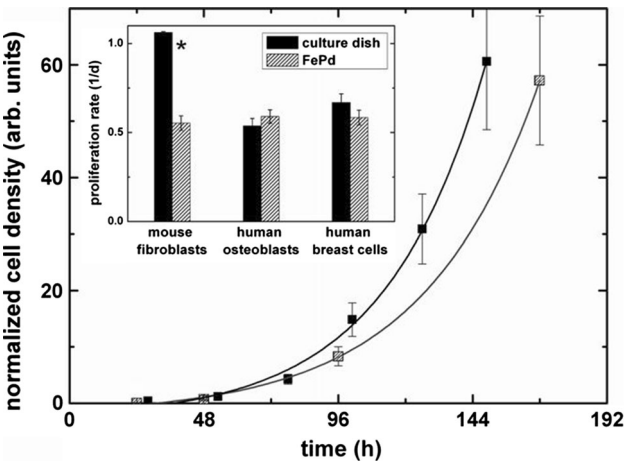

Fig. 16 Growth behavior of MCF-10A epithelial cells (exponential) on Fe–Pd (*gray*) compared with control experiments on cell culture plastic (*black*). *Inset*: proliferation rates for NIH/3T3, HOB and MCF-10A cells on plastic and uncoated Fe–Pd thin films. (Reproduced with permission of Elsevier from Ref. [29]) (Color figure online)

Acknowledgments A. Francis gratefully acknowledges support by the Alexander von Humboldt foundation in form of a fellowship for a research stay for experienced researchers. Ms Yuyun Yang acknowledges a scholarship of the Chinese Scholarship Council.

References

1. Serruys PW, Rensing BJ. Handbook of coronary stents. 4th ed. London: Taylor & Francis; 2001.
2. Tsuji T, Tamai H, Igaki K, Kyo E, Kosuga K, Hata T, Nakamura T, Fujita S, Takeda S, Motohara S, Uehata H. Biodegradable stents as a platform to drug loading. Int J Cardiovasc Interv. 2003;5:13–6.
3. Tsuji T, Tamai H, Igaki K, Kyo E, Kosuga K, Hata T, Okada M, Nakamura T, Komori H, Motohara S, Uehata H. Biodegradable polymeric stents. Curr Interv Cardiol Rep. 2001;3(1):10–7.
4. Huang T, Cheng J, Zheng YF. In vitro degradation and biocompatibility of Fe–Pd and Fe–Pt composites fabricated by spark plasma sintering. Mater Sci Eng. 2014;35:43–53.
5. Moravej M, Mantovani D. Biodegradable metals for cardiovascular stent application: interests and new opportunities. Int J Mol Sci. 2011;12:4250–70.

6. Erbel R, Di Mario C, Bartunek J, Bonnier J, de Bruyne B, Erbeli FR, Erne P, Haude M, Heublein B, Horrigan M, Ilsley C, Bose D, Koolen J, Luscher TF, Weissman N, Waksman R. Temporary scaffolding of coronary arteries with bioabsorbable magnesium stents: a prospective, non-randomized multicentre trial. Lancet. 2007;369:1869–75.
7. Waksman R, Pakala R, Kuchulakanti P, Baffour R, Hellinga D, Seabron R, Tio FO, Wittchow E, Hartwig S, Harder C, Rohde R, Heublein B, Andreae A, Waldmann KH, Haverich A. Safety and efficacy of bioabsorbable magnesium alloy stents in porcine coronary arteries. Catheter Cardiovasc Interv. 2006;68:607–17.
8. Gu X, Zheng Y, Cheng Y, Zhong S, Xi T. In vitro corrosion and biocompatibility of binary magnesium alloys. Biomaterials. 2009;30:484–98.
9. Witte F, Kaese V, Haferkamp H, Switzer E, Meyer-Lindenberg A, Wirth CJ, Windhagen H. In vivo corrosion of four magnesium alloys and the associated bone response. Biomaterials. 2005;26:3557–63.
10. Di Mario C, Griffiths H, Goktekin O, Peeters N, Verbist J, Bosiers M, Deloose K, Heublein B, Rohde R, Kasese V, Ilsley C, Erbel R. Drug-eluting bioabsorbable magnesium stent. J Interv Cardiol. 2004;17:391–5.
11. Auerbach M, Ballard H. Clinical use of intravenous iron: administration, efficacy, and safety. Hematology. 2010;2010:338–47.
12. Ulum MF, Arafat A, Noviana D, Yusop AH, Nasution AK, Abdul Kadir MR, Hermawan H. In vitro and in vivo degradation evaluation of novel iron-bioceramic composites for bone implant applications. Mater Sci Eng. 2014;36:336–44.
13. Wen Z, Zhang L, Chen C, Liu Y, Wu C, Dai C. A construction of novel iron-foam-based calcium phosphate/chitosan coating biodegradable scaffold material. Mater Sci Eng. 2013;33:1022–31.
14. Zhu S, Huang N, Xu L, Zhang Y, Liu H, Sun H, Leng H. Biocompatibility of pure iron: in vitro assessment of degradation kinetics and cytotoxicity on endothelial cells. Mater Sci Eng. 2009;29:1589–92.
15. Peuster M, Hesse C, Schloo T, Fink C, Beerbaum P, von Schnakenburg C. Long-term biocompatibility of a corrodible peripheral iron stent in the porcine descending aorta. Biomaterials. 2006;27:4955–62.
16. Peuster M, Wohlsein P, Brugmann M, Ehlerding M, Seidler K, Fink C, Brauer H, Fischer A, Hausdorf G. A novel approach to temporary stenting: degradable cardiovascular stents produced from corrodible metal-results 6–18 months after implantation into New Zealand white rabbits. Heart. 2001;86:563–9.
17. Hermawan H, Dubé D, Mantovani D. Developments in metallic biodegradable stents. Acta Biomater. 2010;6(5):1693–7.
18. Schinhammer M, Hänzi AC, Löffler JF, Uggowitzer PJ. Design strategy for biodegradable Fe-based alloys for medical applications. Acta Biomater. 2010;6:1705–13.
19. Moszner F, Sologubenkoa A, Schinhammer M, Lerchbacher C, Hänzi A, Leitnerc H, et al. Precipitation hardening of biodegradable Fe–Mn–Pd alloys. Acta Mater. 2011;59:981–91.
20. Schinhammer M, Pecnik C, Rechberger F, Hänzi A, Löffler JF, Uggowitzer PJ. Recrystallization behavior, microstructure evolution and mechanical properties of biodegradable Fe–Mn–C (–Pd) TWIP alloys. Acta Mater. 2012;60:2746–56.
21. Liu B, Zheng YF, Ruan L. In vitro investigation of $Fe_{30}Mn_6Si$ shape memory alloy as potential biodegradable metallic material. Mater Lett. 2011;65:540–3.
22. Wang YB, Li HF, Zheng YF, Li M. Corrosion performances in simulated body fluids and cytotoxicity evaluation of Fe-based bulk metallic glasses. Mater Sci Eng. 2012;32:599–606.
23. Jynge P, Brurok H, Asplund A, Towart R, Refsum H, Karlsson JOG. Cardiovascular safety of MnDPDP and $MnCl_2$. Acta Radiol. 1997;38:740–9.
24. Crossgrove J, Zheng W. Manganese toxicity upon overexposure. NMR Biomed. 2004;17:544–53.
25. Ratner BD. Biomaterials science: an introduction to materials in medicine. Amsterdam, Boston: Elsevier Academic Press; 2004.
26. Callister WD, Rethwisch DG. Materials science and engineering: an introduction. 8th ed. Hoboken: Wiley; 2009.
27. Mitchell BS. An introduction to materials engineering and science for chemical and materials engineers. Hoboken: Wiley; 2004.
28. Liu B, Zheng YF. Effects of alloying elements (Mn Co, Al, W, Sn, B, C and S) on biodegradability and in vitro biocompatibility of pure iron. Acta Biomater. 2011;7:1407–20.
29. Allenstein U, Ma Y, Arabi-Hashemi A, Zink M, Mayr SG. Fe–Pd based ferromagnetic shape memory actuators for medical applications: biocompatibility, effect of surface roughness and protein coatings. Acta Biomater. 2013;9:5845–53.
30. Kock I, Hamann S, Brunken H, Edler T, Mayr SG, Ludwig A. Development and characterization of $Fe_{70}Pd_{30}$ ferromagnetic shape memory splats. Intermetallics. 2010;18(5):877–82.
31. Claussen I, Mayr SG. Mechanical properties and twin boundary drag in FePd ferromagnetic shape memory foils—experiments and ab initio modeling. New J Phys. 2011;13(6):063034.
32. Cheng J, Zheng YF. In vitro study on newly designed biodegradable Fe-X composites (X = W, CNT) prepared by spark plasma sintering. J Biomed Mater Res B. 2013;101B:485–97.
33. Wegener B, Sievers B, Utzschneider S, Peter Müller P, Jansson V, Rößler S, Nies B, Stephani G, Kieback B, Quadbeck P. Microstructure, cytotoxicity and corrosion of powder-metallurgical iron alloys for biodegradable bone replacement materials. Mater Sci Eng. 2011;176:1789–96.
34. Hermawan H, Dubé D, Mantovani D. Degradable metallic biomaterials: design and development of Fe–Mn alloys for stents. J Biomed Mater Res A. 2010;93:1–11.
35. Moravej M, Prima F, Fiset M, Mantovani D. Electroformed iron as new biomaterial for degradable stents: development process and structure–properties relationship. Acta Biomater. 2010;6:1726–35.
36. Nie FL, Zheng YF, Wei SC, Hu C, Yang G. In vitro corrosion, cytotoxicity and hemocompatibility of bulk nanocrystalline pure iron. Biomed Mater. 2010;5:065015.
37. Stolyarov VV, Zhu YT, Lowe TC, Islamgaliev RK, Valiev RZ. A two step SPD processing of ultrafine-grained titanium. Nanostruct Mater. 1999;11(7):947.
38. Serruys PW, Kutryk MJB, Ong ATL. Drug therapy-coronary-artery stents. N Engl J Med. 2006;354:483–95.
39. Hermawan H, Dubé D, Mantovani D. Development of degradable Fe–35Mn alloy for biomedical application. Adv Mater Res. 2007;15(17):107–12 [THERMEC 2006 Supplement].
40. Hermawan H, Alamdari H, Mantovani D, Dube D. Iron–manganese: new class of metallic degradable biomaterials prepared by powder metallurgy. Powder Metall. 2008;51:38–45.
41. Lin HC, Lin KM, Lin CS, Ouyang TM. The corrosion behavior of Fe-based shape memory alloys. Corros Sci. 2002;44:2013–26.
42. Moravej M, Purnama A, Fiset M, Couet J, Mantovani D. Electroformed pure iron as a new biomaterial for degradable stents: in vitro degradation and preliminary cell viability studies. Acta Biomater. 2010;6:1843–51.
43. Schinhammer M, Steiger P, Moszner F, Löffler JF, Uggowitzer PJ. Degradation performance of biodegradable Fe–Mn–C–(Pd) alloys. Mater Sci Eng. 2013;33:1882–93.
44. ASTM G 31-99. Standard practice for laboratory immersion corrosion testing of metals. Conshohocken: ASTM International; 2001.
45. Waksman R, Pakala R, Baffour R, Seabron R, Hellinga D, Tio F. Short-term effects of biocorrodible iron stents in porcine coronary arteries. J Interv Cardiol. 2008;21(1):15–20.
46. Kraus T, Moszner F, Fischerauer S, Fiedler M, Martinelli E, Eichler J, Witte F, Willbold E, Schinhammer M, Meischel M,

Uggowitzer PJ, Löffler JF, Weinberg A. Biodegradable Fe-based alloys for use in osteosynthesis: outcome of an in vivo study after 52 weeks. Acta Biomater. 2014;10:3346–53.
47. Hermawan H, Purnama A, Dube D, Couet J, Mantovani D. Fe–Mn alloys for metallic biodegradable stents: degradation and cell viability studies. Acta Biomater. 2010;6:1852–60.
48. Zhang EL, Chen HY, Shen F. Biocorrosion properties and blood and cell compatibility of pure iron as a biodegradable biomaterial. J Mater Sci Mater Med. 2010;21:2151–63.
49. Schinhammer M, Gerber I, Hänzi AC, Uggowitzer PJ. On the cytocompatibility of biodegradable Fe-based alloys. Mater Sci Eng. 2013;33:782–9.
50. Mueller PP, May T, Perz A, Hauser H, Peuster M. Control of smooth muscle cell proliferation by ferrous iron. Biomaterials. 2006;27:2193–200.
51. Fussenegger M, Bailey JE, Hauser H, Mueller PP. Genetic optimization of recombinant glycoprotein production by mammalian cells. Trends Biotechnol. 1999;17:35–42.
52. Purnama A, Mantovani D, Couet J. Caveolin: a possible biomarker of degradable metallic materials toxicity in vascular cells. Acta Biomater. 2013;9:8754–60.
53. Ma Y, Zink M, Mayr SG. Biocompatibility of single crystalline $Fe_{70}Pd_{30}$ ferromagnetic shape memory films. Appl Phys Lett. 2010;96(21):213703.
54. Food and Nutrition Board Institute of Medicine. Dietary reference intakes for vitamin A, vitamin K, arsenic, boron, chromium, copper, iodide, iron, manganese, molybdenum, nickel, silicon, vanadium, and zinc. Washington: National Academic Press; 2002. p. 290–393.
55. Chen Y, Xu Z, Smith C, Sankar J. Recent advances on the development of magnesium alloys for biodegradable implants. Acta Biomater. 2014;10(11):4561–73.
56. Gu XN, Zheng YF. A review on magnesium alloys as biodegradable materials. Front Mater Sci China. 2010;4:111–5.
57. Mani G, Feldman MD, Patel D, Agrawal CM. Coronary stents: a materials perspective. Biomaterials. 2007;28:1689–710.